Article:

Khamas, S.K. (2009) Electromagnetic radiation by antennas of arbitrary shape in a layered spherical media. IEEE Transactions on Antennas and Propagation, 57 (12). pp. 3827-3834. ISSN 0018-926X

https://doi.org/10.1109/TAP.2009.2033444

Electromagnetic Radiation by Antennas of Arbitrary Shape in a Layered Spherical Media

Salam K. Khamas, *Member, IEEE*

***Abstract*—A unified method of moments model is developed for the analysis of arbitrarily shaped antennas that are radiating next to a multilayered dielectric sphere. The curvilinear Rao-Wilton-Glisson triangular basis functions and dyadic Green's functions have been used in the model. Antennas of various geometries including spherical, circular and rectangular microstrip antennas as well as hemispherical dielectric resonators have been modeled. Input impedance and radiation pattern results are presented and shown to be in good agreement with published data.**

***Index Terms*—Conformal antennas, dyadic Green's function, method of moments (MoM), spherical antennas.**

I. Introduction

ANTENNAS radiating in the proximity of a layered dielectric sphere has been a subject of considerable research studies involving antennas of various configurations, such as conformal microstrip antennas, antennas loaded by a dielectric sphere and antennas that excite hemispherical dielectric resonators. For instance, the radiation characteristics of a probe-fed circular microstrip antenna printed on a layered sphere have been investigated in [1]–[4]. A conformal annular ring patch antenna has been analyzed in [3], [5], [6]. A superstrate loaded spherical antenna has been studied in [7]. Theoretical and experimental studies of spherical arrays have been investigated using rectangular microstrip [8] and stacked circular patch elements [9]. A conformal Archimedean spiral antenna that is printed on a grounded spherical substrate has been presented in [10].

Analysis and measurements of a probe-driven hemispherical dielectric resonator antenna (DRA) have been reported in [11], [12]. A DRA that is excited by a conformal strip has been presented in [13], and a circularly polarized hemispherical DRA that is excited by a conformal parasitic patch has been proposed in [14]. The numerical analyses in [13], [14] have been implemented using novel closed-form expressions in the method of moments (MoM) solution. The input impedance of a monopole loaded by and connected to a perfectly conducting (PEC) sphere has been computed in [15], and the radiation pattern of two monopoles that are connected to a PEC sphere has been presented in [16]. A monopole that is loaded by a DRA has been investigated in [17]. A dipole and helical antennas radiating next to a multilayered dielectric sphere have been reported in [18], [19], with a layered sphere used to model a human head.

In most of the aforementioned studies, the moment method has been adopted in the analysis, where several algorithms have been developed such that each is suitable to efficiently model a number of regular antenna shapes. A unified MoM model that can analyze an arbitrarily, i.e., irregularly or regularly, shaped antenna radiating next to a layered sphere has not been reported earlier. The aim of this study is to introduce a rigorous MoM model that is capable of analyzing spherical antennas of any configuration and substrate thicknesses. This has been achieved by formulating the problem using a mixed potential integral equation (MPIE) for an arbitrarily directed current element in a spherical media. The layered sphere and the antenna have been modeled using dyadic Green's functions [20]–[22] and the well-known curvilinear Rao-Wilton-Glisson (RWG) [23], [24] triangular basis functions respectively. The efficiency of the computation has been enhanced by decomposing dyadic Green's functions into slow and fast convergent components, with the slower convergent elements incorporated into a single scalar potential expression.

To verify the generality and correctness of the presented model, antennas of various shapes have been modeled and analysed, and the results obtained have been compared with results reported in the literature. The investigated geometries include probe fed circular and proximity-coupled rectangular spherical microstrip antennas, where both electrically thin and thick substrates have been considered. The radius, reactance and current distribution of the feeding probe are included in the analysis. A hemispherical dielectric resonator antenna with a radial probe excitation has also been modeled to further verify the accuracy and versatility of the presented model.

II. Theory

A dielectric sphere of N layers is shown in Fig. 1. Each layer has a permittivity of ε_i and a permeability of μ_i with the outermost layer assumed to be free space. The antenna can be positioned arbitrarily in any layer. A perfectly conducting spherical core can be modeled assuming the permeability and permittivity of the innermost layer, that is the N^{th} layer, as $\mu_N \to 0$ and $\varepsilon_N \to \infty$, respectively. Although this assumption is incorrect physically, it is sufficient for numerical modeling purposes as it provides a finite propagation constant in the N^{th} layer [25].

Manuscript received February 09, 2009; revised May 05, 2009. First published October 02, 2009; current version published December 01, 2009.

The author is with the Communications Research Group, Department of Electronic and Electrical Engineering, University of Sheffield, Sheffield S1 3JD, U.K. (e-mail: s.khamas@sheffield.ac.uk).

Color versions of one or more of the figures in this paper are available online at http://ieeexplore.ieee.org.

Digital Object Identifier 10.1109/TAP.2009.2033444

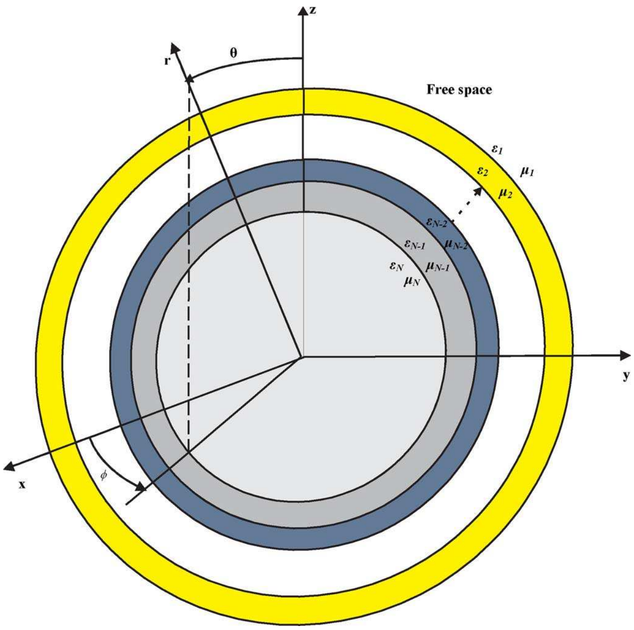

Fig. 1. A layered dielectric sphere.

A. Integral Equation Formulation

The tangential electric field can be obtained using the electric field integral equation (EFIE) or the MPIE, which is more suitable for antennas in layered media. The EFIE is given by [22]

$$\mathbf{E} = -j\omega\mu_f \iint\limits_{s'} \left(\overline{\mathbf{G}}_{0e}\left(\mathbf{r},\mathbf{r}'\right)\delta_f^s + \overline{\mathbf{G}}_{es}^{(fs)}\left(\mathbf{r},\mathbf{r}'\right) \right) \cdot \mathbf{J}(\mathbf{r}')ds' \tag{1}$$

where s' is the surface area of the current source, $\overline{\mathbf{G}}_{0e}\left(\mathbf{r},\mathbf{r}'\right)$ represents the radiation from an antenna located in an infinite homogenous media that can be expressed as [20]

$$\overline{\mathbf{G}}_{0e}\left(\mathbf{r},\mathbf{r}'\right) = \left(\overline{\mathbf{I}} + \frac{1}{k_s^2}\nabla\nabla'\right)\frac{e^{-jk_sR}}{4\pi R} \tag{2}$$

and $\overline{\mathbf{G}}_{es}^{(fs)}\left(\mathbf{r},\mathbf{r}'\right)$ represents the contribution due to the presence of the dielectric sphere, that is

$$\begin{aligned}\overline{\mathbf{G}}_{es}^{(fs)}\left(\mathbf{r},\mathbf{r}'\right) = G_{rr}\hat{\mathbf{r}}\hat{\mathbf{r}} + G_{\theta r}\hat{\boldsymbol{\theta}}\hat{\mathbf{r}} + G_{\phi r}\hat{\boldsymbol{\phi}}\hat{\mathbf{r}} + G_{r\theta}\hat{\mathbf{r}}\hat{\boldsymbol{\theta}} + G_{\theta\theta}\hat{\boldsymbol{\theta}}\hat{\boldsymbol{\theta}} \\ + G_{\phi\theta}\hat{\boldsymbol{\phi}}\hat{\boldsymbol{\theta}} + G_{r\phi}\hat{\mathbf{r}}\hat{\boldsymbol{\phi}} + G_{\theta\phi}\hat{\boldsymbol{\theta}}\hat{\boldsymbol{\phi}} + G_{\phi\phi}\hat{\boldsymbol{\phi}}\hat{\boldsymbol{\phi}}\end{aligned} \tag{3}$$

where the individual components of (3) are given in [22], $k_s = \omega\sqrt{\mu_s\varepsilon_s}$ and the superscript fs refers to the field, $\mathbf{r}\,(r,\theta,\phi)$, and source, $\mathbf{r}'\,(r',\theta',\phi')$, points, respectively. The homogenous media component can be employed only when both of the field and source points are in the same layer. Therefore, when $\mathbf{r}$ and $\mathbf{r}'$ are located at a spherical interface between two layers, the permittivity of either layer can be used to compute this component provided the appropriate $\overline{\mathbf{G}}_{es}^{(fs)}\left(\mathbf{r},\mathbf{r}'\right)$ elements are invoked. As the solution of (2) is well known, it has not been discussed in this article and attention has been given to dyadic Green's functions of (3).

The overall electric field is a superposition of two components: the first represents the fields of the transverse electric (TE) modes and the second represents the fields of the transverse magnetic (TM) modes, where each component is expressed using an infinite summation of spherical harmonics. The convergence of the infinite series depends on a number of factors such as the sphere radius, dielectric permittivities and the locations of the source and observation points [18]. Proper truncation of the summation represents an essential factor in the formulation of a computationally efficient model; hence the series characteristics have been investigated as the summation index, n, approaches infinity, where asymptotic spherical Bessel and Hankel functions expressions have been employed [26]. Such an evaluation has shown that the contribution of TE modes asymptotes to zero for larger n while that of TM modes persists as $n \to \infty$, with an asymptotic behavior that depends on the dielectric properties of the spherical media. Therefore, the summation of the TE modes converges much faster than that of the corresponding TM modes; hence, a considerable improvement in the computation time can be accomplished by incorporating the slowly convergent TM modes components into a unified potential. This can be achieved using a mixed potential integral equation representation of the electric field instead of the EFIE representation in (1). The MPIE can be obtained by introducing a scalar potential that consists of TM modes contributions as well as a magnetic vector potential $\mathbf{A}$. Therefore, (1) may be rewritten as [27]–[29]

$$\mathbf{E} = -j\omega\mathbf{A} - \nabla\psi \tag{4}$$

where

$$\mathbf{A} = \mu_f \iint\limits_{s'} \overline{\mathbf{G}}_{\mathbf{A}} \cdot \mathbf{J}(\mathbf{r}')ds' \tag{5}$$

and the electric scalar potential given by [28]

$$\psi = \iint\limits_{s'} \nabla' G_\psi \cdot \mathbf{J}(\mathbf{r}')ds'. \tag{6}$$

In the case of a conformal current source, that is when there is no radial current component, Green's functions of the electric scalar and magnetic vector potentials can be deduced from (1), (3) as

$$G_\psi = -\frac{\omega\mu_f}{4\pi k_f}\sum_{n=1}^{\infty}\frac{2n+1}{n(n+1)} \cdot \begin{pmatrix} \Delta_1 \frac{d\left(rh_n^{(2)}(k_f r)\right)}{dr}\frac{d\left(r'\zeta_1\right)}{dr'} \\ +\Delta_2 \frac{d\left(rj_n(k_f r)\right)}{dr}\frac{d\left(r'\zeta_2\right)}{dr'} \end{pmatrix} P_n(\cos\gamma) \tag{7}$$

and

$$\overline{\mathbf{G}}_{\mathbf{A}} = G_{\theta\theta}^A\hat{\boldsymbol{\theta}}\hat{\boldsymbol{\theta}} + G_{\theta\phi}^A\hat{\boldsymbol{\theta}}\hat{\boldsymbol{\phi}} + G_{\phi\theta}^A\hat{\boldsymbol{\phi}}\hat{\boldsymbol{\theta}} + G_{\phi\phi}^A\hat{\boldsymbol{\phi}}\hat{\boldsymbol{\phi}} \tag{8}$$

where

$$G_{\theta\theta}^A = \frac{\partial^2\psi_{TE}}{\sin\theta\sin\theta'\partial\phi'\partial\phi} \tag{9}$$

$$G^A_{\theta\phi} = -\frac{\partial^2 \psi_{TE}}{\sin\theta \partial\phi \partial\theta'} \tag{10}$$

$$G^A_{\phi\theta} = -\frac{\partial^2 \psi_{TE}}{\sin\theta' \partial\phi' \partial\theta} \tag{11}$$

$$G^A_{\phi\phi} = \frac{\partial^2 \psi_{TE}}{\partial\theta' \partial\theta} \tag{12}$$

$$\psi_{TE} = -\frac{jk_s}{4\pi} \sum_{n=1}^{\infty} \frac{2n+1}{n(n+1)} \begin{pmatrix} \Delta_1 h_n^{(2)}(k_f r)\zeta_3 \\ +\Delta_2 j_n(k_f r)\zeta_4 \end{pmatrix} \cdot P_n(\cos\gamma). \tag{13}$$

Therefore, for a conformal current element, there are four magnetic vector potential entries that represent the contribution of the TE modes and a single scalar potential that represents the TM modes contribution.

In the equations above

$$\begin{aligned} \zeta_1 &= a_n^{TM} j_n(k_s r')\Delta_3 + b_n^{TM} h_n^{(2)}(k_s r')\Delta_4 \\ \zeta_2 &= c_n^{TM} j_n(k_s r')\Delta_3 + d_n^{TM} h_n^{(2)}(k_s r')\Delta_4 \\ \zeta_3 &= a_n^{TE} j_n(k_s r')\Delta_3 + b_n^{TE} h_n^{(2)}(k_s r')\Delta_4 \\ \zeta_4 &= c_n^{TE} j_n(k_s r')\Delta_3 + d_n^{TE} h_n^{(2)}(k_s r')\Delta_4 \end{aligned} \tag{14}$$

where $\Delta_1 = \left(1-\delta_f^N\right)$, $\Delta_2 = \left(1-\delta_f^1\right)$, $\Delta_3 = \left(1-\delta_s^1\right)$, $\Delta_4 = \left(1-\delta_s^N\right)$, δ_u^v is the Kronecker delta, $P_n(\cos\gamma)$ is the Legendre function of degree n, $\cos\gamma = \cos\theta\cos\theta' + \sin\theta\sin\theta'\cos(\phi-\phi')$, $j_n(kr)$ is the spherical Bessel function and $h_n^{(2)}(kr)$ is the spherical Hankel function of the second type. The TE and TM modes expansion coefficients $a_n^{TE,TM}$, $b_n^{TE,TM}$, $c_n^{TE,TM}$ and $d_n^{TE,TM}$ are given in [22].

In the presence of a radial current source, the scalar potential ψ is still applicable as long as a correction term is incorporated into each of the magnetic vector potential components that are associated with a radial current source, that is

$$\begin{aligned} \overline{\mathbf{G}}_{\mathbf{A}} = {} & G^A_{rr}\hat{\mathbf{r}}\hat{\mathbf{r}} + G^A_{\theta r}\hat{\boldsymbol{\theta}}\hat{\mathbf{r}} + G^A_{\phi r}\hat{\boldsymbol{\phi}}\hat{\mathbf{r}} + G^A_{r\theta}\hat{\mathbf{r}}\hat{\boldsymbol{\theta}} + G^A_{\theta\theta}\hat{\boldsymbol{\theta}}\hat{\boldsymbol{\theta}} \\ & + G^A_{\phi\theta}\hat{\boldsymbol{\phi}}\hat{\boldsymbol{\theta}} + G^A_{r\phi}\hat{\mathbf{r}}\hat{\boldsymbol{\phi}} + G^A_{\theta\phi}\hat{\boldsymbol{\theta}}\hat{\boldsymbol{\phi}} + G^A_{\phi\phi}\hat{\boldsymbol{\phi}}\hat{\boldsymbol{\phi}} \end{aligned} \tag{15}$$

and

$$G^A_{rr} = \left(G_{rr} - \frac{1}{j\omega\mu_f}\frac{\partial^2 G_\psi}{\partial r \partial r'}\right) \tag{16}$$

$$G^A_{\theta r} = \left(G_{\theta r} - \frac{1}{j\omega\mu_f}\frac{\partial^2 G_\psi}{r\partial\theta \partial r'}\right) \tag{17}$$

$$G^A_{\phi r} = \left(G_{\phi r} - \frac{1}{j\omega\mu_f}\frac{\partial^2 G_\psi}{r\sin\theta\partial\phi \partial r'}\right) \tag{18}$$

$$G^A_{r\theta} = \left(G_{r\theta} - \frac{1}{j\omega\mu_f}\frac{\partial^2 G_\psi}{r'\partial\theta' \partial r}\right) \tag{19}$$

$$G^A_{r\phi} = \left(G_{r\phi} - \frac{1}{j\omega\mu_f}\frac{\partial^2 G_\psi}{r'\sin\theta'\partial\phi' \partial r}\right) \tag{20}$$

where the first terms in (16)–(20) involve the EFIE dyadic Green's function elements G_{rr}, $G_{\theta r}$, $G_{\phi r}$, $G_{r\theta}$ and $G_{r\phi}$ that are given explicitly in [22]. Substitution of (7), (15) into (4) results in a consolidated model that can be used to analyze arbitrarily directed current elements at the vicinity of a multilayered sphere.

In this study, the infinite summations of the $\overline{\mathbf{G}}_{\mathbf{A}}$ elements have been truncated using 60 terms, while the summation of G_ψ has been truncated using 180 terms. As there are nine entries for $\overline{\mathbf{G}}_{\mathbf{A}}$, a considerable reduction in the computation time has been achieved by merging the slower convergent electric field components into a unified scalar potential. The aforementioned truncation limits have been used to ensure that convergence is achieved for all the presented structures. A typical computation time for a spherical microstrip antenna with 250 unknowns is 6 seconds per frequency point on a 2 GHz Pentium dual processor.

B. MOM Solution

Equation (4) has been solved using the method of moments, where the antenna surface has been divided into a mesh of curvilinear triangular patches as shown in Fig. 2(a). The parametric coordinates ξ_1, ξ_2 and ξ_3 have been used to transform the curvilinear triangle into a planar triangle as shown in Fig. 2(b). The curvilinear RWG triangular basis functions [24] are defined over two triangles that share a common interior edge. These functions have been employed in this study and they are expressed as [24], [30], [31]

$$\begin{aligned} \boldsymbol{\Lambda}_1(\mathbf{r}) &= \frac{1}{\sqrt{g}}\left(\xi_2\frac{\partial\mathbf{r}}{\partial\xi_2} - \xi_2\frac{\partial\mathbf{r}}{\partial\xi_1} - \xi_3\frac{\partial\mathbf{r}}{\partial\xi_1}\right) \\ \boldsymbol{\Lambda}_2(\mathbf{r}) &= \frac{1}{\sqrt{g}}\left(\xi_1\frac{\partial\mathbf{r}}{\partial\xi_1} - \xi_3\frac{\partial\mathbf{r}}{\partial\xi_2} - \xi_1\frac{\partial\mathbf{r}}{\partial\xi_2}\right) \\ \boldsymbol{\Lambda}_3(\mathbf{r}) &= \frac{1}{\sqrt{g}}\left(\xi_1\frac{\partial\mathbf{r}}{\partial\xi_1} + \xi_2\frac{\partial\mathbf{r}}{\partial\xi_2}\right) \end{aligned} \tag{21}$$

where the subscripts refer to the local edge number in a triangle, $\mathbf{r}$ is the position vector from the global coordinate origin to any point on the curvilinear triangle that is given by [30]

$$\begin{aligned} \mathbf{r} = {} & \xi_1(2\xi_1-1)\mathbf{r}_1 + \xi_2(2\xi_2-1)\mathbf{r}_2 + \xi_3(2\xi_3-1)\mathbf{r}_3 \\ & + 4\xi_1\xi_2\mathbf{r}_4 + 4\xi_2\xi_3\mathbf{r}_5 + 4\xi_3\xi_1\mathbf{r}_6 \end{aligned} \tag{22}$$

and $\sqrt{g}$ is the Jacobian at $\mathbf{r}$. The position vectors $\mathbf{r}_1$, $\mathbf{r}_2$ and $\mathbf{r}_3$ define the vertices of a curvilinear triangular patch, while $\mathbf{r}_4$, $\mathbf{r}_5$ and $\mathbf{r}_6$ denote the midpoints of the triangle's three edges as shown in Fig. 2. The surface current density can then be expressed as

$$\mathbf{J}(\mathbf{r}') = \sum_{q=1}^{N_q} I_q \boldsymbol{\Lambda}_q(\mathbf{r}') \tag{23}$$

where the subscripts denote an interior edge number, N_q is the total number of non-boundary edges in the mesh that can be calculated as [23]

$$N_q = \frac{3N_f - N_b}{2} \tag{24}$$

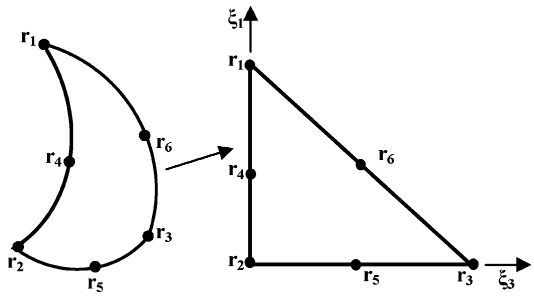

Fig. 2. (a) Curvilinear triangle in the Cartesian coordinates. (b) Equivalent planar triangle in the parametric coordinates ξ_1, ξ_2 and ξ_3.

in which N_f represents the total number of triangular patches and N_b is the number of boundary edges. Substituting (23) in (4)–(6) provides an alternative expression of the electric field as

$$\mathbf{E} = \sum_{q=1}^{N_q} I_q \mathbf{E}_q \tag{25}$$

where

$$\mathbf{E}_q = -\iint_{s'} \left[j\omega\mu_f \overline{\mathbf{G}}_{\mathbf{A}} \cdot \boldsymbol{\Lambda}_q(\mathbf{r}') + \boldsymbol{\nabla}\left(\boldsymbol{\nabla}' G_\psi \cdot \boldsymbol{\Lambda}_q(\mathbf{r}')\right)\right] ds'. \tag{26}$$

The impedance matrix elements have been calculated using Galerkin's MoM as [32]

$$Z_{pq} = \iint_{s} \boldsymbol{\Lambda}_p(\mathbf{r}) \cdot \mathbf{E}_q ds \tag{27}$$

which gives

$$Z_{pq} = -\iint_{s} \iint_{s'} \begin{bmatrix} j\omega\mu_f \boldsymbol{\Lambda}_p(\mathbf{r}) \cdot \overline{\mathbf{G}}_{\mathbf{A}} \cdot \boldsymbol{\Lambda}_q(\mathbf{r}') \\ +(\boldsymbol{\nabla} \cdot \boldsymbol{\Lambda}_p(\mathbf{r}))G_\psi(\boldsymbol{\nabla}' \cdot \boldsymbol{\Lambda}_q(\mathbf{r}')) \end{bmatrix} ds' ds \tag{28}$$

where p and q refer to the test and expansion edges and $\boldsymbol{\nabla} \cdot \boldsymbol{\Lambda} = 2/\sqrt{g}$ [24]. In deriving (28), the divergence theorem has been employed to transfer the differential operators $\boldsymbol{\nabla}$ and $\boldsymbol{\nabla}'$ of (26) to act on the testing and expansion current functions which results in a smoother integral. The integration over the testing triangle surface has been avoided by using the approximate Galerkin method [23], in which testing can be implemented at the centroid of a curvilinear triangle. The surface integral over the source triangle has been computed using symmetric quadrature rules over the unit triangle [33].

A problem that needs special attention is the connection of a feeding probe to the perfectly conducting spherical core; this is particularly important for the rigorous analysis of a probe-fed spherical microstrip antenna. A possible solution is to model the probe as a strip of width w that is equivalent to four times the probe radius [34]. The common edge between the PEC sphere and the probe should follow the curvature of the sphere precisely as illustrated in Fig. 3. To eliminate any convergence problems at this attachment, an image of the probe above an infinite PEC planar ground plane has been introduced in the solution. The dyadic Green's function of this image has been expressed as a summation of spherical harmonics, subtracted from the spherical dyadic Green's function and then added, in closed form, to the homogenous media component of the Green's function, that is (2) [35].

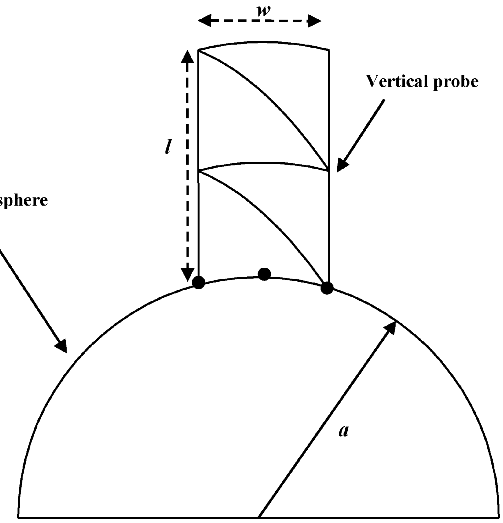

Fig. 3. A monopole strip attached to a PEC sphere.

The far-field components have been determined from the computed current distribution using the asymptotic expressions of Hankel's functions when $r \to \infty$, that is, $h_n^{(2)}(k_o r) = j^{n+1}(e^{-jk_o r}/k_o r)$ and $\partial\left(r h_n^{(2)}(k_o r)\right)/\partial r = j^n e^{-jk_o r}$. The infinite summation has been truncated using 40 terms in the far-field computation.

III. Results

In this section, the validity and generality of the presented algorithm has been verified for several geometries, where good agreements between computed and published results have been achieved in all cases.

Each conformal antenna is driven using a probe that is connected to the PEC spherical core. A delta gap voltage source has been used in the analysis where it has been placed at the base of the feeding probe. Rigorous analysis of the probe has been employed as it facilitates the inclusion of the probe's length, radius and reactance in the computations. To connect the probe to the conformal patch a probe-patch junction needs to be included in the model. Such a junction is introduced by the double use of the edge shared by the probe and the patch, that is, the common edge is declared twice in the mesh [36].

A. Spherical Circular Microstrip Antenna

A circular patch that is printed on and in conformance with a layered sphere is shown in Fig. 4. An example that has been studied by several researchers [1], [3] is analyzed using a PEC spherical core of 5 cm radius, $\varepsilon_{r2} = 1$, a spherical substrate of $\varepsilon_{r3} = 2.47$ and a 0.32 cm thickness, i.e., the overall sphere radius of Fig. 4 is 5.32 cm. The conformal patch has an arc radius of 1.88 cm and the excitation probe is positioned at an arc distance of 0.94 cm from the antenna center. The probe

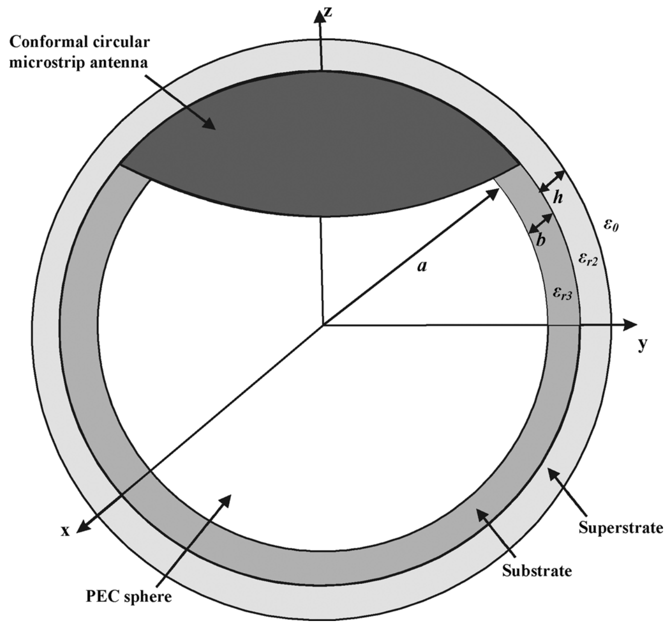

Fig. 4. A conformal circular microstrip antenna printed on a layered sphere.

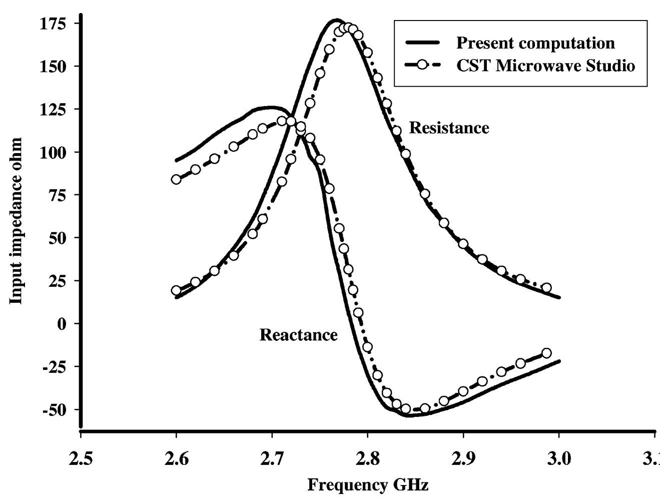

Fig. 5. The input impedance of a spherical circular microstrip antenna.

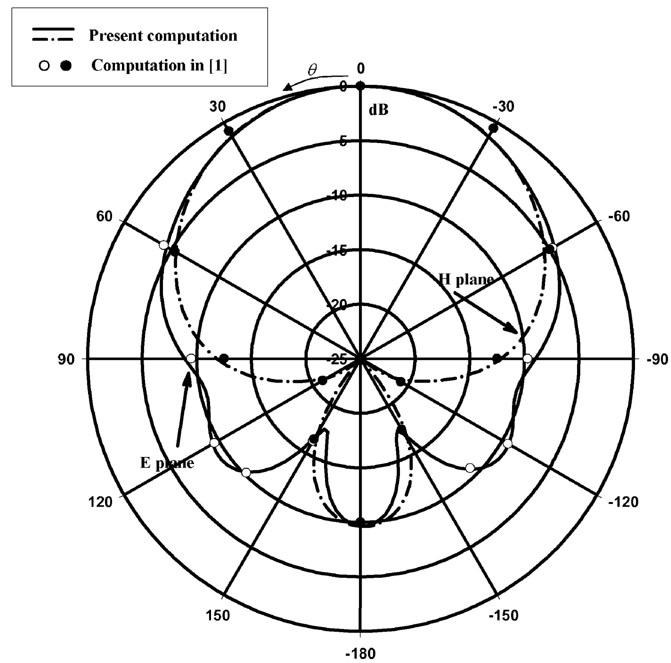

Fig. 6. Radiation pattern of a spherical circular microstrip antenna.

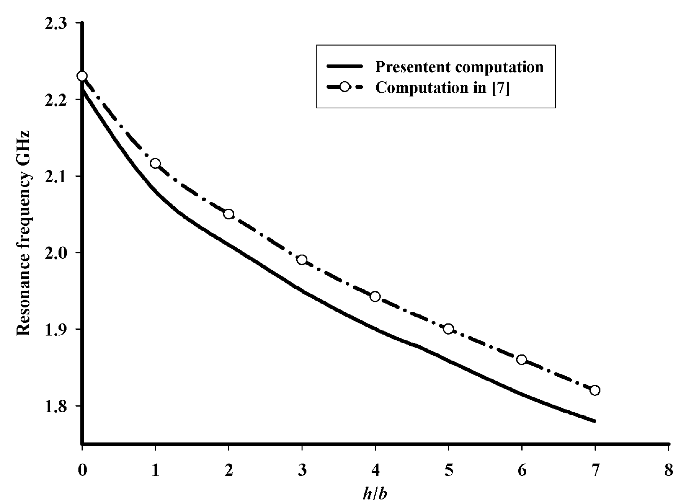

Fig. 7. The resonance frequency of a spherical circular microstrip antenna as a function of superstrate thickness.

width has been chosen as $w = 0.2$ cm, which is equivalent to a coaxial probe of 0.05 cm radius. A convergent solution has been achieved when the antenna surface is meshed into 176 curvilinear triangles in addition to two triangles on the probe, resulting in a total of 248 interior edges.

The input impedance of this antenna has been calculated then compared with that obtained using CST microwave studio [37]. The results are in good agreement as shown in Fig. 5, where the probe radius and length have been included in both solutions. The computation time of the MoM model is 3 minutes for all frequency points compared to several hours using CST over a frequency range of 2.6 to 3 GHz. The E-plane and H-plane far-field patterns have been calculated using the aforementioned patch parameters with a different substrate thickness of 0.16 cm as shown in Fig. 6. Comparison with the results reported in [1] validates the accuracy of the present computation.

The presence of a spherical superstrate has been investigated using a PEC spherical core with a radius of 5 cm and a circular patch with an arc radius of 2.5 cm. The substrate has a relative permittivity of $\varepsilon_{r3} = 2.5$ and a thickness of 0.1588 cm. The excitation probe has been placed at an arc distance of 1.64 cm from the antenna center. Fig. 7 illustrates the variation of the resonance frequency as a function of the superstrate thickness when $\varepsilon_{r2} = 8.2$. The computed resonance frequencies agree well with those reported in [7] with a slight discrepancy of 2% that could be attributed to the probe's reactance. The resonance frequency has been defined as the frequency at which the reactive component of the input impedance is zero.

B. Spherical Patch Proximity FED by a Conformal L-Shaped Probe

Fig. 8 presents a conformal patch printed on a grounded spherical foam substrate with a relative permittivity of 1. A conformal L-shaped probe is connected to the PEC spherical

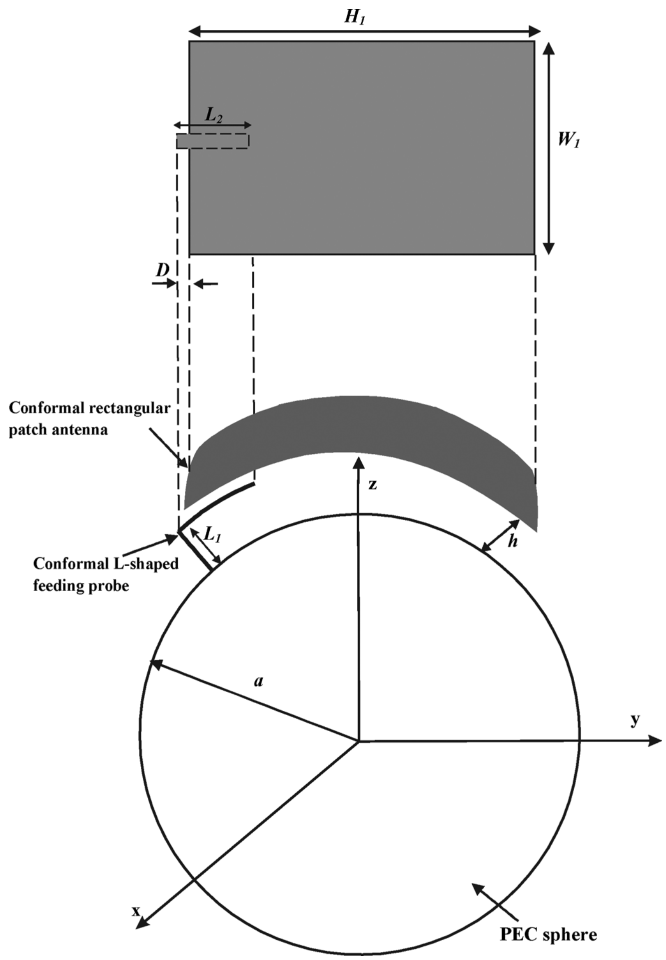

Fig. 8. A spherical rectangular patch antenna proximity fed by a conformal L-shaped probe.

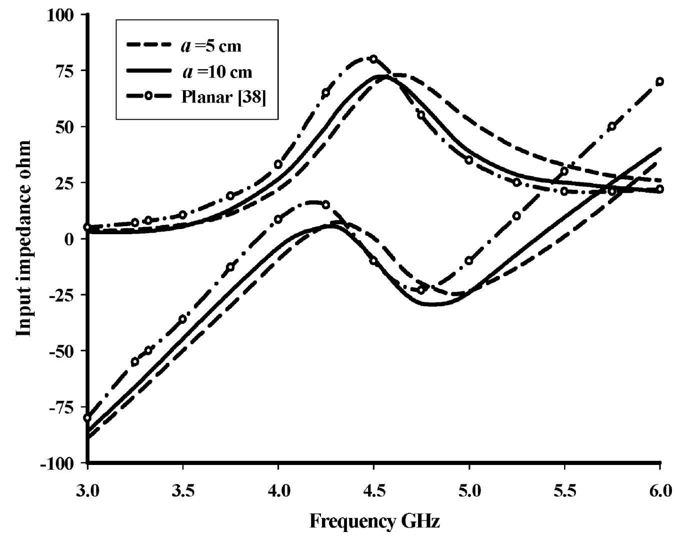

Fig. 9. Input impedance of a proximity coupled spherical rectangular patch antenna.

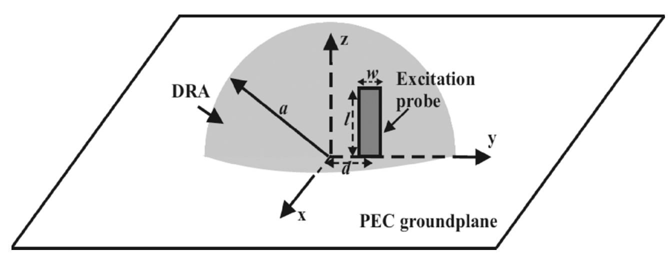

Fig. 10. Hemispherical dielectric resonator antenna excited by a vertical probe.

core. This example is based on a planar antenna structure presented in [38], where a flat patch was placed above a grounded foam substrate and excited using a coupling from an L-shaped probe. The dimensions of this antenna are similar to those reported in [38], that is $W_1 = 3$ cm, $H_1 = 2.5$ cm, $L_1 = 0.495$ cm, $L_2 = 1$ cm, $D = 0.2$ cm and $h = 0.66$ cm. The feeding probe has been modeled as a strip of 2 mm width. The surfaces of the patch and probe have been meshed into 84 and 8 curvilinear triangles, respectively, resulting in 121 unknowns for a convergent MoM solution. The input impedance of the spherical patch antenna is shown in Fig. 9 compared to that of the planar antenna given in [38]. It can be seen that the impedance and resonance frequency of the spherical antenna approach that of the planar counterpart for a larger PEC sphere radius. Therefore, a higher resonance frequency is expected as the curvature of the structure is increased.

C. Hemispherical Dielectric Resonator Antennas

A probe-fed DRA is illustrated in Fig. 10. This antenna has been analyzed following an example reported in [11] using a probe length of $l = 1.52$ cm, a dielectric hemisphere of a 2.54 cm radius and a relative permittivity of 8.9. The cylindrical probe has a radius of 0.75 mm and it is shifted from the origin by a distance of $d = 1.74$ cm. In this study the cylindrical probe has been replaced by a planar strip of width 3 mm. The presence of the planar PEC groundplane has been simulated using the image theory, that is, the problem is modeled using a full dielectric sphere excited by a center-fed strip of length $2l$. The surface of the strip has been meshed into 20 curvilinear triangles, which results in 19 unknowns. The calculated input impedance of this structure is shown in Fig. 11, which indicates that the results achieved using the presented method agree well with those reported in [11].

IV. Conclusion

This article has introduced a MoM model that can analyze the radiation characteristics of arbitrarily shaped antennas when a layered dielectric sphere is present. The computation efficiency has been enhanced by merging the slowly convergent electric field components into an electric scalar potential that needs to be computed once for each curvilinear triangular patch. The configurations presented have been chosen to illustrate the flexibility and generality of the presented model in the analyses of antennas for various applications, where conformal and dielectric resonator antennas have been studied. The robustness and accuracy of the model has been verified by comparing the computed results with those available in the literature. In the study, low-order RWG basis functions have been used, which could be replaced by the higher-order interpolatory bases functions [31] to improve the convergence and computation efficiency of the solution. The presented analysis can be enhanced further by

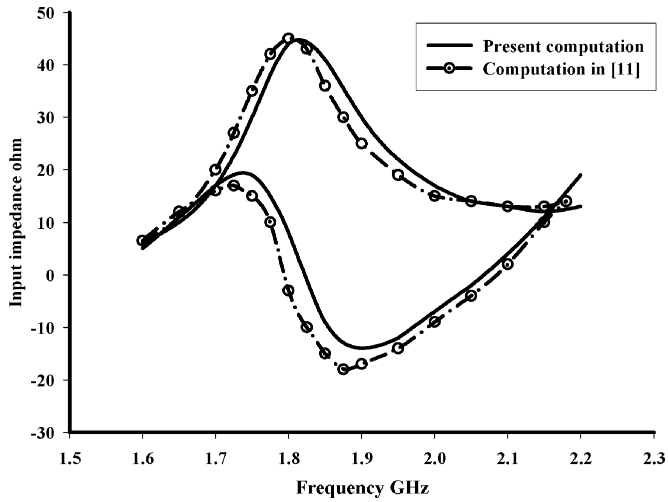

Fig. 11. The input impedance of a probe fed hemispherical DRA.

employing a coaxial feeding probe model, which can be incorporated into the formulation using a special attachment basis function that facilitates the connection of a cylindrical wire to the vertex of a curvilinear triangular patch [39], [40].

ACKNOWLEDGMENT

The helpful and constructive comments of the reviewers are greatly appreciated.

REFERENCES

[1] B. Ke and A. A. Kishk, "Analysis of spherical circular microstrip antenna," *Proc. Inst. Elect. Eng.*, vol. 138, pt. H, pp. 542–548, Dec. 1991.
[2] W. Y. Tam and K. M. Luk, "Far field analysis of spherical-circular microstrip antennas by electric surface current models," *Proc. Inst. Elect. Eng.*, vol. 138, pt. H, pp. 98–102, Feb. 1991.
[3] W. Y. Tam, A. K. Y. Lai, and K. M. Luk, "Input impedance of spherical microstrip antenna," *Proc. Inst. Elect. Eng.*, vol. 142, pt. H, pp. 285–288, Jun. 1995.
[4] H. T. Chen and K. L. Wong, "Analysis of a probe-fed spherical circular microstrip antennas using cavity-model theory," *Microw. Opt. Technol. Lett.*, vol. 7, pp. 309–312, May 1994.
[5] A. A. Kishk, "Analysis of spherical annular microstrip antennas," *IEEE Trans. Antennas Propag.*, vol. 41, pp. 338–343, Mar. 1993.
[6] H. T. Chen, H. D. Chen, and Y. T. Chen, "Full-wave analysis of a disk loaded spherical annular-ring microstrip antenna," *Micow. Opt. Tech. Lett.*, vol. 12, pp. 353–358, Aug. 1996.
[7] K. L. Wong, S. F. Hsiao, and H. T. Chen, "Resonance and radiation of a superstrate loaded spherical-circular microstrip patch antenna," *IEEE Trans. Antennas Propag.*, vol. 41, pp. 686–690, May 1993.
[8] Z. Sipus, N. Burum, S. Skokic, and P. S. Kildal, "Analysis of spherical arrays of microstrip antennas using moment method in spectral domain," *Proc. Inst. Elect. Eng.*, vol. 153, pt. H, pp. 533–543, Dec. 2006.
[9] Z. Sipus, S. Skokic, M. Bosiljevac, and N. Burum, "Study of mutual coupling between circular stacked-patch antennas on a sphere," *IEEE Trans. Antennas Propag.*, vol. 56, pp. 1834–1844, Aug. 2008.
[10] S. K. Khamas, "Moment method analysis of an Archimedean spiral printed on a layered dielectric sphere," *IEEE Trans. Antennas Propag.*, vol. 56, pp. 345–352, Feb. 2008.
[11] A. A. Kishk, G. Zltou, and A. W. Glisson, "Analysis of dielectric-resonator antennas with emphasis on hemispherical structures," *IEEE Antennas Propag. Mag.*, vol. 36, pp. 20–31, Apr. 1994.
[12] K. W. Leung, K. M. Luk, K. Y. A. Lai, and D. Lin, "Theory and experiment of a coaxial probe fed hemispherical dielectric resonator antenna," *IEEE Trans. Antennas Propag.*, vol. 41, pp. 1390–1398, Oct. 1993.
[13] K. W. Leung, "Conformal strip excitation of dielectric resonator antenna," *IEEE Trans. Antennas Propag.*, vol. 48, pp. 961–967, Jun. 2000.
[14] K. W. Leung and H. K. Ng, "Theory and experiment of circularly polarized dielectric resonator antenna with a parasitic patch," *IEEE Trans. Antennas Propag.*, vol. 51, pp. 405–412, Mar. 2003.
[15] F. M. Tesche, A. R. Neureuther, and R. E. Stovall, "The analysis of monopole antennas located on a spherical vehicle: Part 2, Numerical and experimental results," *IEEE Trans. Electromagn. Compat.*, vol. 18, pp. 8–15, Feb. 1976.
[16] F. M. Tesche and A. R. Neureuther, "Radiation patterns for two monopoles on a perfectly conducting sphere," *IEEE Trans. Antennas Propag.*, vol. 8, pp. 692–694, Sep. 1970.
[17] K. K. Tse, K. W. Leung, K. M. Luk, and E. K. N. Yung, "A monopole antenna loaded by a hemispherical dielectric resonator," *IEEE Trans. Antennas Propag.*, vol. 51, pp. 413–420, Mar. 2003.
[18] K. S. Nikita, G. S. Stamatakos, N. K. Uzunoglun, and A. Karafotias, "Analysis of the interaction between a layered spherical human head model and a finite-length dipole," *IEEE Trans. Microw. Theory Tech.*, vol. 48, pp. 2003–2013, Nov. 2000.
[19] S. Koulouridis and K. S. Nikita, "Study of the coupling between human head and cellular phone helical antennas," *IEEE Trans. Electromagn. Compat.*, vol. 46, pp. 62–70, Feb. 2004.
[20] C. T. Tai, *Dyadic Green's Functions in Electromagnetics Theory*. Scranton, PA: Intext Educational, 1971.
[21] W. C. Chew, *Waves and Fields in Inhomogeneous Media*. New York: Van Nostrand, 1990.
[22] L. W. Li, P. S. Kooi, M. S. Leong, and T. S. Yeo, "Electromagnetic dyadic Green's function in spherically multilayered media," *IEEE Trans. Microw. Theory Tech.*, vol. 42, pp. 2302–2310, Dec. 1994.
[23] S. M. Rao, D. R. Wilton, and A. W. Glisson, "Electromagnetic scattering by surfaces of arbitrary shape," *IEEE Trans. Antennas Propag.*, vol. 30, pp. 409–418, May 1982.
[24] S. Wandzura, "Electric current basis functions for curved surfaces," *Electromagnetics*, vol. 12, pp. 77–91, Jan. 1992.
[25] R. F. Harrington, *Time Harmonic Electromagnetic Fields*. New York: Mc Graw-Hill, 1961.
[26] M. Abramowitz and I. A. Stegun, *Handbook of Mathematical Functions with Formulas, Graphs, and Mathematical Tables*. Washington, DC: Government Printing Office, 1964.
[27] K. A. Michalski and D. Zheng, "Electromagnetic scattering and radiation by surfaces of arbitrary shape in layered media, Part I: Theory," *IEEE Trans. Antennas Propag.*, vol. 38, pp. 335–344, Mar. 1990.
[28] K. A. Michalski, "Formulation of mixed potential integral equations for arbitrarily shaped microstrip structures with uniaxial substrates," *J. Electromagn. Waves Applicat.*, vol. 7, pp. 899–917, Jul. 1993.
[29] J. Sun, C. F. Wang, L. W. Li, and M. S. Leong, "Mixed potential spatial domain Green's functions in fast computational form for cylindrically stratified media," *Progr. Electromagn. Res.*, vol. 45, pp. 181–199, 2004.
[30] W. C. Chew, J. M. Jin, E. Michielssen, and J. Song, *Fast and Efficient Algorithms in Computational Electromagnetics*. Boston, MA: Artech House, 2001.
[31] R. D. Graglia, D. R. Wilton, and A. F. Peterson, "Higher order interpolatory vector bases for computational electromagnetics," *IEEE Trans. Antennas Propag.*, vol. 45, pp. 329–342, Mar. 1997.
[32] W. L. Stutzman and G. A. Thiele, *Antenna Theory and Design*. New York: Wiley, 1981.
[33] E. Akin, *Finite Elements for Analysis and Design*. London, U.K.: Academic Press, 1994.
[34] C. Butler, "The equivalent radius of a narrow conducting strip," *IEEE Trans. Antennas Propag.*, vol. AP-30, no. 7, pp. 755–758, Jul. 1982.
[35] B. D. Milovanovic, "Numerical analysis of radial thin-wire antenna in presence of conducting sphere," *Elect. Lett.*, vol. 16, no. 15, pp. 611–612, Jul. 1980.
[36] A. Apte and S. Makarov, "Execution times for the solution of MoM equations in Matlab," in *Proc. IEEE Antennas Propag. Int. Symp.*, Jun. 2002, vol. 1, pp. 692–695.
[37] CST Reference Manual. Darmstadt, Germany, Computer Simulation Technology, 2008.
[38] Y. X. Guo, C. L. Mak, K. M. Luk, and K. F. Lee, "Analysis and design of L-probe proximity fed patch antennas," *IEEE Trans. Antennas Propag.*, vol. 49, pp. 145–149, Feb. 2001.
[39] S. U. Hwu, D. R. Wilton, and S. M. Rao, "Electromagnetic scattering and radiation by arbitrary conducting wire-surface configuration," in *IEEE APS Int. Symp. Dig.*, Jun. 1988, vol. 2, pp. 890–893.
[40] H. Y. Chao, J. Zhao, and W. C. Chew, "Application of curvilinear basis functions and MLFMA for radiation and scattering problems involving curved PEC structures," *IEEE Trans. Antennas Propag.*, vol. 51, pp. 331–336, Feb. 2003.

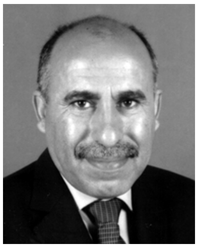

Salam K. Khamas (M'04) received the B.Sc. degree in electronic engineering from the University of Technology, Baghdad, Iraq, and the Ph.D. degree from the University of Sheffield, Sheffield, U.K., in 1985 and 1992 respectively.

From 1993 to 1998, he worked as a Research Associate in the Electronic and Electrical Engineering Department, Sheffield University. From 1998 to 2002, he was a Software Engineer in Alcatel Telecommunications and then in Nortel Networks. Since 2002, he has been a Lecturer in the Electronic and Electrical Engineering Department, University of Sheffield. His research interests include computational electromagnetics, conformal antennas, frequency independent antennas, array design and dielectric resonator antennas.